A Consequent-Pole Hybrid Exciter for Synchronous Generators

Stefano Nuzzo, *Member, IEEE*, Paolo Bolognesi, *Member, IEEE*, Giovanni Decuzzi, Paolo Giangrande, *Member, IEEE,* Michael Galea, *Senior Member, IEEE*

***Abstract*-- In low-to-medium power generating sets, a self-powered brushless excitation system is typically employed. This solution is cost-effective, simple and compact, but it suffers from an unreliable voltage build-up at start-up, a slow dynamic response and a relatively low efficiency for the exciter. The push towards more effective, reliable and efficient products has recently led to consider excitation systems equipped with permanent magnet exciters and controlled rotating converters, but they are still considered too complex and costly. This paper investigates the utilization of a hybrid excitation for the exciter, aiming to join the benefits of field windings and permanent magnets. As a case study, this concept is applied to an industrial generating set. After a preliminary analysis, a consequent-pole layout with surface-mounted bonded magnets is selected as the most effective solution in an industrial perspective, since it permits to maximize the benefits while minimizing the required modifications in the system design. Theoretical considerations, numerical analysis and experimental validation are reported to show that the hybrid excitation concept can actually lead to a significant reduction of the exciter field losses as well as to other appreciable side benefits with a limited impact on the generating set design.**

I. Introduction

THE general trend in the design of electrical machines is presently towards more efficient, power-dense and reliable solutions. This has determined a growing interest also in renewing and revamping the design of classical machines such as wound-field synchronous generators (WFSGs) [1]-[4].

Apart from their traditional role, i.e. grid-connected electrical generation in large power plants [5], WFSGs are also very important in small-to-medium power generating sets (gensets) intended for isolated operations and/or standby/emergency applications [2]. In these applications, self-sufficiency, robustness, commissioning simplicity, minimal maintenance requirements and low cost are key features. These characteristics are matched nowadays pretty well by the popular brushless excitation system (ES), which is then by far the most preferred choice. Its typical configuration comprises a 3-phase inverted-layout auxiliary WFSG used as exciter, whose stationary field winding is supplied and controlled by an automatic voltage regulator (AVR). The rotating armature of the exciter supplies a rotating full-bridge diode rectifier that feeds in turn the field winding of the main alternator (MA), which is a WFSG featuring a conventional layout and typically a 3-phase armature. While this architecture is widely used, it was recently shown that some aspects (e.g. the voltage drop ensuing from the diode commutations [6]) are still overlooked, thus often resulting in over-engineered exciters [7]. Other drawbacks of the conventional brushless ES include: a) the AVR is supplied by the armature of the MA (i.e. the system is self-excited) and is therefore inherently affected by its operative conditions, especially during large transients [8]; b) during the start-up process of the genset, the voltage build-up only relies upon the residual magnetism in the rotor core, thus resulting relatively slow and not fully reliable.

To overcome such drawbacks, especially in mid-large gensets a pilot exciter, whose excitation is provided by permanent magnets (PMs), is often added to supply the AVR as soon as the genset rotates at its minimum design speed. However, this solution leads to a larger, heavier and more expensive system. Recently, the use of PMs directly for the main exciter has been proposed to eliminate the pilot exciter. However, such solution entails the replacement of the passive diode rectifier with some sort of actively controlled converter [9] to permit adjusting the field winding current of the MA. Besides allowing to eliminate the Joule losses in the exciter field winding, combining PM exciters and rotating controlled converters may provide some additional benefits compared to the classical scheme. These include a faster dynamic response, a reduced ripple in the current fed to the MA field winding and an improved controllability. Nevertheless, most manufactures are still reluctant to adopt significant variations in the traditional designs of small-to-medium-size genset, due to their higher complexity and production cost.

This paper investigates a different solution consisting in using an exciter featuring a hybrid excitation, i.e. equipped with both PMs and field winding. The proposed concept is applied for upgrading the existing exciter of an industrial genset, which is presented as a case study. A hybrid-excited machine joins the benefits of both the main categories of ESs above recalled, i.e. 1) based on wound-field exciters and diode rectifiers (like the case study) and 2) based on PM exciters and controllable converters. In fact, on one hand it maintains the high compactness, the low system complexity and limited

S. Nuzzo is with the Department of Engineering Enzo Ferrari, University of Modena and Reggio Emilia, Modena, Italy (e-mail: stefano.nuzzo@unimore.it) and with the Power Electronics, Machines and Control Group, University of Nottingham, Nottingham, UK (e-mail: stefano.nuzzo@nottingham.ac.uk).

P. Bolognesi is with the Electric Machines, Power Electronics and Drives group of the Department DESTEC, University of Pisa, Pisa, Italy (e-mail: p.bolognesi@ieee.org).

G. Decuzzi was with the University of Pisa, Italy, on leave at the University of Nottingham, UK (e-mail: giovanni.decuzzi2@positech.it).

P. Giangrande and Michael Galea are with the Power Electronics, Machines and Control Group, University of Nottingham, Nottingham, UK (e-mail: p.giangrande@nottingham.ac.uk and michael.galea@nottingham.ac.uk).

M. Galea is also with the Power Electronics, Machines and Control Group, University of Nottingham Ningbo, Ningbo, China (e-mail: michael.galea@nottingham.edu.cn).

production costs typical of the first category, while featuring a fully reliable voltage build-up (thanks to the embedded PMs) without requiring an additional pilot exciter. On the other hand, it achieves a significant reduction of the exciter field losses as in the second category, without requiring a controllable converter interposed between exciter and MA (thanks to the field winding regulation capability).

Neither the hybrid excitation [10], [11], nor the consequent-pole arrangement [12], nor the combination of these two features [13] are new concepts by themselves, as they have been proposed in the past. Nevertheless, the hybrid excitation concept has never been applied to exciters of small-to-medium gensets, where indeed it could result in several advantages.

II. Proposed Concept

In Fig. 1, the block scheme of the genset considered as case study is illustrated. It comprises a $400kVA$, $400V$, $50Hz$, 3-phase salient-pole MA and a conventional brushless ES composed of a wound-field exciter, a rotating diode rectifier and an AVR.

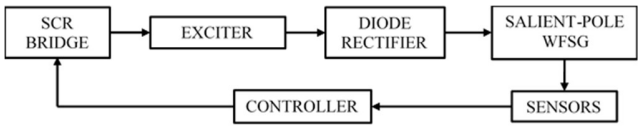

Fig. 1. Architecture of the industrial genset considered as case study.

The focus of this paper is on the exciter, which is a 3-phase inverted-layout rotating-armature WFSG designed to provide $\approx 5kW$ to the field winding of the MA when it operates at rated load. The exciter field winding is wound around the stator poles, whereas the armature coils are deployed in a single-layer layout resulting in a simple full-pitch, 1 slot-per-pole-per-phase winding arrangement. To feed and regulate the average current in the exciter field winding, the AVR is equipped with a single-phase, half-wave controlled rectifier consisting of 1 SCR and 1 diode in anti-parallel to the load to provide a freewheeling path for the MA field current when the SCR is blocked. The main parameters of the MA and of the exciter are listed in Table I, for the sake of completeness.

TABLE I
Main parameters of Alternator and Exciter

	Alternator	Exciter
Rated Power [kVA]	400	5.35
Line-to-line rated Voltage [$Vrms$]	400	75
Rated Frequency [Hz]	50	175
Pole Number	4	14
Armature Slot Number	48	42
Magnetic Laminations	M700-65A	M700-65A
Field winding resistance @20°C [Ω]	1.35	18

The key idea investigated in this paper consists in using the PMs to provide an appropriate "basic level" in the excitation flux of the exciter and thus in the current provided to the MA field winding, while the capability to regulate the value of such current is still fully retained by properly adjusting the field current of the exciter, similarly to classical brushless ESs. Depending on the application, any operating condition of the MA could be selected for defining such basic level and thus for sizing accordingly the PMs.

The industrial genset considered in this paper is designed to operate only supplying widely variable ohmic-inductive passive loads at rated voltage and frequency (and thus speed). In such conditions, the armature reaction in the MA always produces a voltage drop, meaning that the field current required to keep the output voltage at its rated value is always greater or equal than that producing such voltage at no load. In turn, this implies that the excitation flux in the exciter never falls below the value required to reach the rated voltage of the MA at no-load. Hence, the most convenient choice consists in sizing the PMs in such a way that, when the field current in the exciter is zero and no load is connected to the MA, its output voltage assumes the rated value. This allows to keep unmodified the converters presently used in the benchmark genset, i.e. both the rotating diode bridge and the unidirectional SCR-based rectifier in the AVR, thus limiting the modifications with respect to the benchmark genset.

III. Analysis of the Benchmark Exciter

Aiming to pave the way for the accurate design of the PM - field winding machine, it is deemed essential to develop and validate a finite-element (FE) model for the benchmark exciter. In this section, the FE model of the benchmark exciter is then detailed and the relevant results are compared to the experimental ones. Once the validity of the FE model is confirmed, it is slightly updated before being used for the hybrid exciter design.

A. Simulation Model

In the considered case study, the axial length of the exciter is $50mm$ whereas the external diameter is $500mm$, giving a rather low 1:10 ratio, which suggests to keep into account the end effects. Rather than building up a 3D model, which would be computationally expensive, the analysis can be carried out via a 2D FE model coupled with an auxiliary circuital part, where the active sides of the modeled coils (labeled *Coil_S* and *Coil_R* for stator and rotor windings respectively in the scheme depicted in Fig. 2, which refers to the considered case study) can be properly connected each other and to any other circuital element eventually required. In particular, resistive and inductive elements can be included in the circuit to emulate the end effects, i.e. mainly the extra leakage fluxes and resistive voltages and losses. Therefore, the 3D end effects were modelled via the circuital part accompanying the 2D FE model. Accordingly, these phenomena are taken into account by adding in the circuit some appropriate resistors (R_{S_3D} and R_{R_3D} for stator and rotor respectively) and inductors (L_{S_3D} and L_{R_3D} for stator and rotor respectively) as shown in Fig. 2. The values of such elements were estimated according to [14] and can be found in [7] for the exciter under analysis.

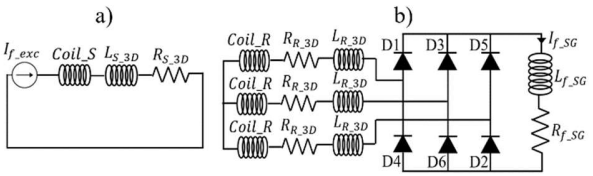

Fig. 2. Circuit coupled to the 2D FE model of the exciter: a) stator b) rotor

According to the specific operating condition to be simulated, and considering the way the related experimental tests were performed, either a current or a voltage DC source

was used to feed the exciter field winding. In Fig. 2, the example with a constant current generator is reported.

Regarding the load fed by the exciter through the rotating rectifier, in reality it consists of the field winding of the MA. The MA field winding can be represented as an ohmic-inductive series load composed of the equivalent resistance R_{f_SG} and self-inductance L_{f_SG}, as observed in Fig. 2. However, if the real value of the self-inductance of the MA field winding was used (i.e. $\approx 4H$ for the considered case study), a large time constant L_{f_SG}/R_{f_SG} would be obtained (about 3s), thus requiring a very long time to achieve steady-state. Therefore, after a sensitivity analysis aimed at finding an optimal trade-off between accuracy and computation burden, a simplified representation was adopted consisting in modeling the MA field winding as an ideal constant current generator, whose value is chosen coherently with the operative conditions targeted.

Concerning the FE model itself, the 14-poles odd-symmetric structure of the machine was exploited by modeling only an angular sector corresponding to 1 pole pitch. A 2D cross section of the FE model developed for the benchmark exciter is shown in Fig. 3, featuring 1 coil side per each armature phase in the rotor as well as the field coil obtained by merging for simplicity the 2 actual coil sides wound around the 2 adjacent stator poles.

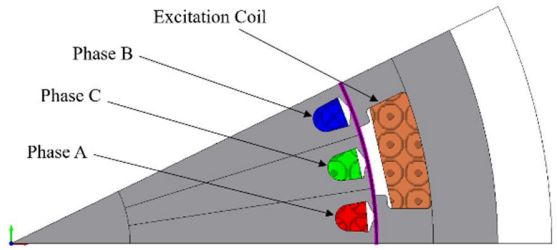

Fig. 3. 2-D FE model of the benchmark exciter (1/14 of the whole machine).

B. Simulation results and experimental validation

The precursor of the FE model adopted in this paper was already validated in [7]. Hereafter, additional comparisons between simulation results and experimental data obtained under corresponding conditions are presented to further prove the validity of the model also for the sake of this investigation.

First, the no-load voltages generated at rated speed ($1500rpm$) at the exciter armature terminals (i.e. with the MA field winding disconnected from the rectifier DC output) for a significant value of field current (i.e. $1A$) are compared in Fig. 4 in terms of waveforms and related low-frequency amplitude spectrum. A very good match between simulation and experimental results can be observed.

A second comparison is performed when the genset rotates at rated speed and the exciter field current is set to an appropriate value ($0.64A$) such that the rotating rectifier feeds the MA field winding with the DC current ($14.6A$) producing the rated line-to-line voltage ($400Vrms$) at no load. The voltage waveforms obtained from simulations and measurements in such conditions at the DC output of the rotating rectifier are compared in Fig. 5. A very good agreement is observed in terms of both average values ($21.8V$ FE vs. $21.2V$ experimental) and overall trend, thus confirming the FE model validity.

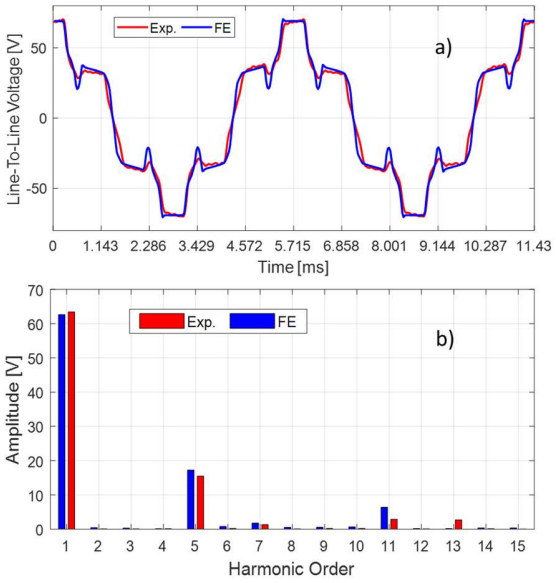

Fig. 4. Comparison between FE and experimental line-to-line armature voltages generated by the benchmark exciter at rated speed ($1500rpm$) with null phase currents and field current equal to 1A: a) waveforms, b) spectra.

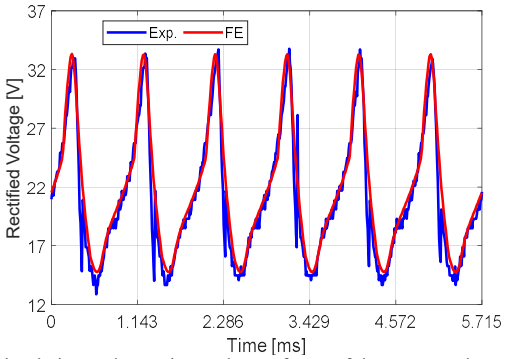

Fig. 5. Simulation and experimental waveforms of the output voltage provided by the rotating rectifier at rated speed under MA no-load rated voltage operation with exciter and alternator field currents equal to $0.64A$ and $14.6A$ respectively.

IV. Design of the Hybrid Exciter

In this section, the design procedure of the hybrid PM – field winding exciter is presented. First, preliminary design considerations and constraints are presented. Then, the validated FE model above recalled is updated to include the PMs and is used to analyze a number of possible design solutions aiming to identify the optimal one. The steps leading to the final selection of a consequent-pole hybrid-excited topology are then detailed.

A. Preliminary design considerations and constraints

Given the typical industrial context of the considered class of gensets, a main constraint for any realistic upgrade project consists in minimizing any disruptive modification compared to the present design of the benchmark ES and, in general, of the whole system. The following guidelines, based on geometrical, economical and operational considerations, were then assumed for the design of the hybrid exciter:

1) the rotor was kept identical to the benchmark exciter;
2) the thickness of the mechanical airgap was maintained the same as in the benchmark exciter ($1mm$);

3) the stator was kept identical to the benchmark exciter, apart from including the features required to host the PMs. A surface-mounted layout was then chosen, assuming to glue the PMs onto the gap-facing surface of the pole shoes;
4) the PM material was wisely selected to minimize the impact on the production costs;
5) the overall design had to be able to reduce the excitation power required at any condition in the considered operation range, i.e. in over-excitation mode from null up to full load.

B. Analytical sizing

Having identified the design constraints, as well as the location and layout of the PMs, the sizing procedure can begin aiming to produce the same value of airgap flux density as in the benchmark machine at the selected "basic supply" condition, i.e. the rated no-load operation of the MA. Therefore, the airgap flux density relative to both benchmark and hybrid exciters needs to be evaluated first. Then, the imposition of the equality condition between the flux densities will allow determining the preliminary size of the PMs.

According to [15], in the airgap of any rotating machine equipped with surface-mounted PMs, the average radial flux density B_G can be related to the magnetic field strength H_G via the constitutive equation (1), where $\bar{\imath}$ is the vector of currents entering the machine phases, α is the angular position of rotor vs. stator, λ is a normalized coordinate mapping the whole airgap along the tangential direction, μ_0 is the permeability of vacuum. According to (2), H_G can be determined as the ratio of the equivalent magneto-motive force (m.m.f.) F_E to the equivalent airgap thickness ε_E given in (3).

$$B_G(\lambda, \alpha, \bar{\imath}) = \mu_0 \, H_G(\lambda, \alpha, \bar{\imath}) \tag{1}$$

$$H_G(\lambda, \alpha) = \frac{F_E(\lambda, \alpha, \bar{\imath})}{\varepsilon_E(\lambda, \alpha)} \tag{2}$$

$$\varepsilon_E(\lambda, \alpha) = \varepsilon_G(\lambda, \alpha) + \varepsilon_M(\lambda, \alpha) \frac{r_G(\lambda, \alpha)}{r_M(\lambda, \alpha)} \frac{\mu_0}{\mu_M} \tag{3}$$

In (3), μ_M is the relative permeability of the PMs; $\varepsilon_G(\lambda,\alpha)$ and $\varepsilon_M(\lambda,\alpha)$ are functions providing the magnetic thickness of the mechanical airgap and of the PMs, respectively; $r_G(\lambda,\alpha)$ and $r_M(\lambda,\alpha)$ are the radii of the mean magnetic surfaces inside the mechanical airgap and the PMs, respectively. Therefore, in the benchmark exciter $\varepsilon_E(\lambda,\alpha)=\varepsilon_G(\lambda,\alpha)$ since no PMs are present.

When the same "basic supply" operating condition is desired for both the hybrid and the benchmark machines, the same airgap flux density levels should be achieved. The equivalent value of stator m.m.f. is given in the benchmark exciter by the product of the equivalent field winding function $N_{exc}(\lambda,\alpha)$ by the field current I_{exc}. In the hybrid exciter, the field current is null for the considered basic condition, meaning that only the PMs provide a contribution to the equivalent m.m.f. This is given by the product of their virtual coercive force H_{CB} by their thickness $\varepsilon_M(\lambda,\alpha)$. Therefore, (4) can be obtained by imposing the equality between the $B_G(\lambda,\alpha,\bar{\imath})$ expressions determined for both exciters.

$$\frac{N_{exc}(\lambda, \alpha) \, I_{exc}}{\varepsilon_G(\lambda, \alpha)} = \frac{H_{cB} \, \varepsilon_M(\lambda, \alpha)}{\varepsilon_G(\lambda, \alpha) + \varepsilon_M(\lambda, \alpha) \frac{r_G(\lambda, \alpha)}{r_M(\lambda, \alpha)} \frac{\mu_0}{\mu_M}} \tag{4}$$

In (4), the left side is well known as it refers to the benchmark exciter. The parameters to be selected for the design of the hybrid exciter are therefore $H_{cB}(\lambda,\alpha)$, $\varepsilon_M(\lambda,\alpha)$ and $r_M(\lambda,\alpha)$, which are related to the PMs. In particular, the first two quantities are mostly significant, since the third one will be dominated by the fixed bore diameter assumed for the stator structure.

C. First design of the hybrid exciter

Given the need of minimizing the equivalent airgap, a thickness of 0.5*mm* was initially considered for the PMs, leading to a uniform equivalent airgap thickness of about 1.5*mm*. Assuming that all stator poles are equipped with a layer of PMs featuring the same thickness and same coercive field with radial magnetization, (4) permits to estimate the required value of H_{cB} in the range of 500-600*kA/m*. These values are compatible with low-end and bonded variants of Samarium-Cobalt (SmCo) and Neodymium-Iron-Boron (NdFeB) rare-earth materials. To such purpose, the FE model validated for the benchmark exciter was updated to include the PMs, keeping all of the major features described in Section III.A.

Although the above analysis showed very promising results in the whole range of operating conditions of the MA, a preliminary assessment of the practical feasibility of the designed solution, involving inquiring manufacturers of PMs, highlighted some challenges. In fact, the very thin non-standard thickness assumed for the PMs (0.5*mm*) turned out to be challenging to manufacture. Therefore, the PM thickness was increased up to the minimum value suggested by the manufactures, i.e. 1*mm*. Accordingly, the resulting value of H_{cB} was reduced to ≈300-400*kA/m*, i.e. compatible also with high-end hard ferrites, but in the end such materials were ruled out as still difficult to manufacture in such a thin thickness. On the other hand, from a thermal point of view, temperatures in the order of 60°*C* were experimentally recorded in the benchmark exciter field winding during rated full-load operation of the MA, thus excluding any need for PMs able to operate at high temperature. Therefore, SmCo was also ruled out.

Bonded NdFeB magnets (BNP-6 type) with a radial thickness of 1*mm* were then finally selected, featuring the properties listed in Table II. It is worth noting that the high electric resistivity featured by such material confirms that the eddy currents inside the PMs may be neglected for the sake of this investigation.

TABLE II
Main Properties of Selected Bonded NdFeB Material

Remanence Br [T]	0.55-0.62	Temp. Coeff. of H_{cJ} $\alpha(H_{cJ})$ [%/°K]	-0.35
Coercivity H_{cB} [kA/m]	285-370	Recoil Permeability μ_{rec}	1.15
Intrinsic Ceorcivity H_{cJ} [kA/m]	600-755	Curie Temperature T_c [°C]	300
Average Resistivity [mΩcm]	5.6	Max. Operating Temp. T_w [°C]	130

The designed solution was checked first via FE analysis, aiming to confirm that the selected "basic supply" condition was correctly achieved. Therefore, the MA rated no-load condition was examined with the exciter field current set to zero (i.e. the PMs contribution only was considered). The results revealed that the rectifier output voltage waveform is very similar to that of the benchmark genset, plotted in red in Fig. 5, yet with average value ≈4% lower. While this first check was passed, some drawbacks due to the increased equivalent magnetic airgap were highlighted. In fact, in such a

configuration, the equivalent airgap thickness becomes ≈2*mm* (1*mm* mechanical airgap + 1*mm* PMs) and the FE analysis showed a ≈6% increase in the exciter field current required to support the MA full-load rated operation.

D. Final consequent-pole configuration of the hybrid exciter

Relying on the above results, to reduce the negative effect of the equivalent gap increase in the hybrid exciter, a promising solution was singled out by adopting a consequent-pole surface-mounted PM layout [13], which consists in mounting PMs only on one stator pole in each pair (e.g. only the North-oriented), whereas the other 7 poles are left unaltered as in the benchmark machine. Therefore, the basic excitation target was reduced to permit using such inexpensive PMs, i.e. some field current will be required even to obtain the rated voltage output from the MA at rated speed and no-load. However, in the end, this choice could be convenient as long as it permits to appreciably reduce the m.m.f. required to the field winding in any MA condition. This was then reputed to be the most suitable choice for the considered case study, using the same PMs previously selected.

E. Simulation model and results for the proposed exciter

Since the consequent-pole layout of the hybrid exciter is not significantly different from the structures previously analyzed, the considerations presented in Section III.A are still applicable, meaning that a 2D FE model with associated circuital part is suitable to analyze also the proposed machine. On the other hand, the latter does not feature an odd-periodic symmetrical layout as the benchmark exciter. Therefore, in this case the even-periodic symmetry related to the 7 existing pole pairs dictates the minimum extension of the modeled region, i.e. 2 pole pitches. The geometry of the 2-D FE model of the proposed consequent-pole structure is reported in Fig. 6, where an in-zoom of a stator tooth hosting a PM (in yellow) is also highlighted. All of the major features of the circuital part are kept the same as in Fig. 2b.

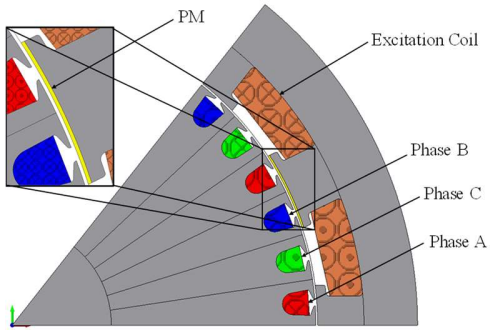

Fig. 6. 2-D cross section of the consequent-pole hybrid exciter FE model (1-7th of the whole machine).

In Fig. 7, the field maps related to 4 different operating conditions of the hybrid exciter at rated speed are reported in the same shaded colors scale: a) no current fed to the rectifier; b) no-load, rated output voltage for the MA; c) 50% of loading of the MA at rated voltage; d) full rated condition of the MA. A very small difference is observed between a) and b) conditions, meaning that the armature reaction effect in the exciter is negligible at the selected "basic supply" operating point. A more significant effect is seen in Figures 8c and 8d, but even at full-load the impact of the armature reaction on the magnetic conditions is limited. Further results provided by the FE model are presented in Section V in comparison with experimental data obtained from a purposely-built full-scale prototype.

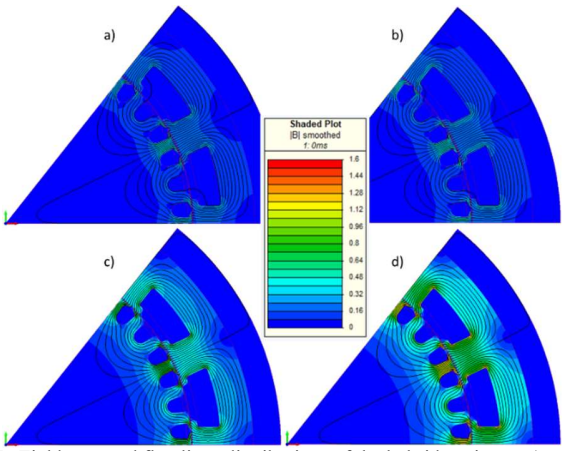

Fig. 7. Field map and flux lines distributions of the hybrid exciter at a) no-load operation of the exciter, b) rated no-load condition of the MA, c) 50% of loading of the MA at rated voltage and d) rated full-load operation of the MA.

F. Temperature influence and demagnetization analysis

While the simulations above recalled were carried out assuming cold conditions (environment temperature, i.e. 20°C) for the genset, the proper operation of the proposed hybrid excitation was also verified considering the degradation of the PM properties at the rated operating temperature of the exciter (i.e. 60°C). The performance curves for the selected PM material are shown in Fig. 8 for different temperatures. The equivalent linearized PM properties at 60° were estimated by using the temperature coefficient listed in Table II. Given its the relatively low value and the modest temperature rise ΔT=40°C, no major difference was spotted in the results compared to the cold condition scenario.

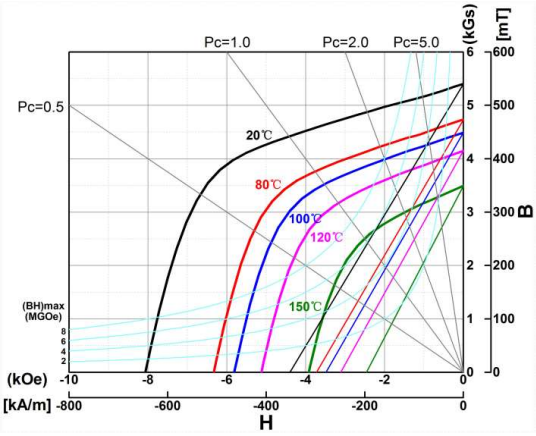

Fig. 8. Demagnetization curves at various temperatures of the selected bonded NdFeB PMs (BNP-6 type).

In addition, the risk of demagnetization of the PMs due to excessive reverse field was assessed under critical operating conditions. The real PM demagnetization curves are linear for the whole range of temperatures reported in the figure, meaning that the demagnetization knee is located in the third quadrant. This is also obviously true for the curve at 60°, although the latter is not shown in the figure.

Referring to the curves in Fig. 8, the value of the P_c ratio between magnet and airgap thicknesses is approximately equal to 1 in the considered design. When current flows in the exciter

field winding, with a direction always aimed to increase the flux density to compensate for the voltage drops due to the armature reaction, the operating point of the PMs is pushed even further back from the demagnetization knee. To further support the above conclusions, FE simulations were carried out at both full-load and short-circuit conditions, using the PM properties related to 60°C. The "demagnetization prediction" tool provided by the FE software was then used to spot any potential related risk. As expected, such a risk was not highlighted at any simulated time instant in both of the examined conditions.

V. Prototyping and Experimental Validation

A. Prototype

Aiming to minimize any discrepancy with respect to the considered benchmark genset, a consequent-pole hybrid machine was manufactured by simply modifying an available specimen. The gap-facing surface of 1 stator pole in each pair was then properly milled to host the PMs.

With the aim to simplify the assembly procedure, save on purchase costs and also further reduce the potential for eddy currents losses in the PMs, the volume of magnet planned to be used in each modified stator pole was segmented into 8 identical arc-shaped PMs arranged in a 2 axial x 4 tangential array layout. Therefore, a total of 8x7=56 individual PMs were required, each one featuring an axial length equal to 25*mm*, an angular span of 3.71° and a radial thickness of 1*mm*, with outer radius equal to 170.5*mm*. A picture comparing one of them to a coin is provided in Fig. 9a, highlighting its handy format.

The PMs were then glued onto the machined gap-facing surfaces using an appropriate commercial epoxy resin. In Fig. 9b, an overview of the resulting stator arrangement is reported, whereas Fig. 9c shows a zoom-in view of 3 teeth highlighting the consequent-pole layout adopted.

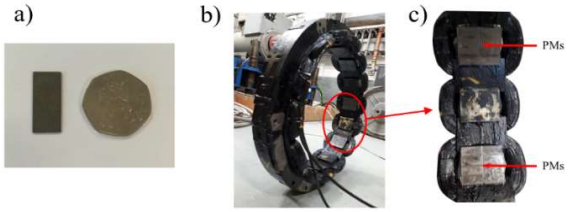

Fig. 9. Prototype exciter: a) Arc-shaped bonded NdFeB PM, b) exciter stator after milling and gluing of the PMs, c) zoom-in on 3 stator teeth.

B. Experimental platform

After completion of the hybrid exciter stator prototype, it was assembled back into the available industrial genset that it had been taken from. The modified genset was then installed onto a test rig to permit investigating its operation, getting the experimental setup sketched in Fig. 10. The MA was mechanically coupled via a 10*kNm* torque-speed transducer to an 800*kW* induction machine (IM), which was properly supplied by a dedicated drive fed by the power grid to make it operate as the prime mover in either speed- or torque-control modes. The MA armature was also electrically connected to the power grid via a suited contactor, permitting to carry out both no-load tests when left open and on-load tests when closed, thus implementing the power recirculation test concept. A set of brushes and slip rings was also purposely installed at the back of the genset to permit both to disconnect at will the MA field winding from the rotating rectifier output and to record the most significant quantities related to the rotating windings, i.e. the line-to-line output voltages of the exciter and the voltage and current of the MA field winding. A general overview of the experimental test bench is shown in Fig. 11.

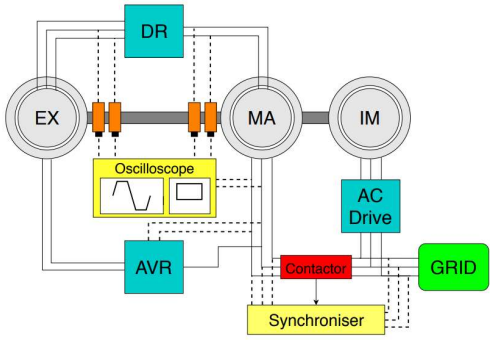

Fig. 10. Schematic of the experimental setup.

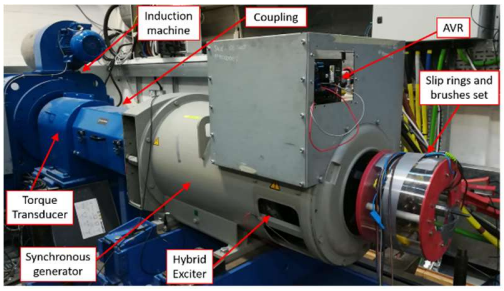

Fig. 11. Overview of the experimental setup.

C. Experimental tests

The hybrid exciter prototype was characterized by performing 3 types of tests, as detailed below.

1) No-load operation of the exciter. In this test, the genset speed is kept at the rated value 1500*rpm* by the induction drive operating in speed-control mode. The exciter field winding current is fed and adjusted by a DC power supply operating in current control mode, whereas its armature currents are null since the field winding of the MA is disconnected from the rotating rectifier output. The AVR and the MA armature winding are also left open. In these conditions, the line-to-line armature voltage generated by the exciter and the related DC output voltage provided by the rectifier are measured.
2) No-load operation of the MA. In this test, the genset speed is still kept at its rated value by the induction drive operating in speed-control mode. The MA armature winding is left open, whereas its field winding is connected to the output of the rotating rectifier. The field current in the MA, and thus its no-load armature voltage, are then controlled indirectly by adjusting the field current in the exciter, which is still provided by the DC power supply operating in current-control mode. The exciter AC voltage and the MA field voltage and current are measured, as well as the MA armature voltage. The AVR is left unused.
3) On-load operation of the MA. The induction drive initially accelerates the genset up to the rated speed while the AVR provides the field current to the exciter monitoring the armature voltages of the MA. When all the conditions for grid connection are satisfied, the synchronizer closes the contactor to permit the MA working as generator feeding power to the mains. The induction drive is simultaneously switched to torque-control mode and its torque is then properly settled to operate the MA under different active

load conditions. The AVR is switched to its secondary operation mode, acting as an adjustable power factor (p.f.) controller by regulating the exciter field current. Besides all the measurements listed for test type 2), output power, voltage, current and p.f. of the MA are also recorded.

The experimental data obtained from the above tests are presented and commented in the next sub-sections.

D. Model validation

A first significant check concerns the line-to-line voltage generated by the exciter at rated speed and null armature currents (i.e. no-load operation supported only by the PMs – test type 1). The corresponding voltage waveforms and low-frequency amplitude spectra provided by the simulation model and by the experimental tests are compared in Fig. 12.

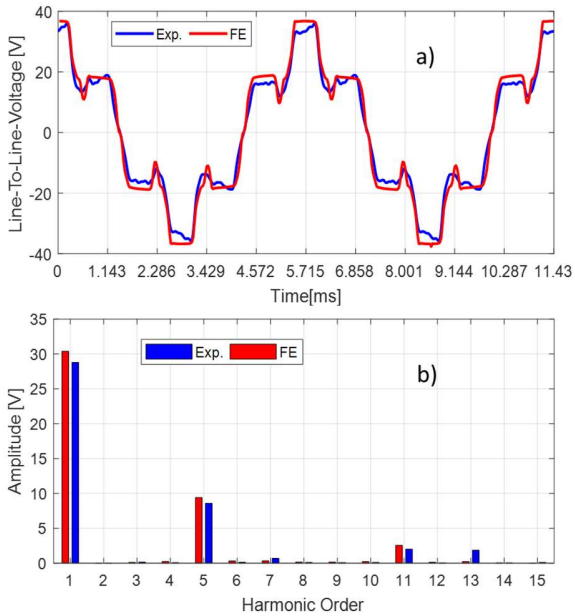

Fig. 12. Comparison between FE and experimental line-to-line voltage waveforms provided by the hybrid exciter at rated speed 1500*rpm* when its armature current is null: a) waveforms, b) spectra.

Overall, a good match is observed, despite some minor discrepancies. These might be due to a number of reasons, including slight differences in the B-H curves of cores' and PMs' materials. In fact, the slight overestimation seen in the FE results compared to the experimental ones of Fig. 12 is confirmed by observing the comparison shown with continuous lines in Fig. 13, where the field current is increased from 0*A* to 3.2*A* to obtain the exciter no-load curve. This leads to conclude that, likely, the PMs properties provided and set within the FE model overrate the real magnets' performance. Nevertheless, the relative error never exceeds 4.5% at any field current value. For the sake of compactness, in Fig. 13, also the on-load results of the hybrid exciter are reported. The comparison between FE results and experimental measurements is provided in terms of p.u. line-to-line voltage for several significant operating conditions of the MA, i.e. 0%, 25%, 50%, 75%, 100% and 110% of the rated load with inductive p.f. equal to 0.8. Given the good agreement observed, the accuracy of the simulation model is therefore further validated.

Among these MA loading levels, the 0% case, corresponding to the no-load operation of the MA at rated speed and voltage, is the most significant for the sake of this study, as it represents the "basic supply" operating point selected for the sizing of the PMs. Hence, for such operating condition, simulation results and experimental data concerning the average field current and the rms armature voltage of the MA are compared for 2 levels of exciter field current, i.e. zero and a value that makes the MA generate approximately its rated voltage. The simulation results related to the MA field current were obtained via the model described in Section IV.E, whereas the corresponding output voltage values were obtained by using such current values in the 2D FE model of the same machine built for a previous investigation [2]. Overall, in Table III, a very good agreement is observed between numerical and experimental results. As expected, when the exciter field current is null, the MA output voltage at no load is somewhat lower than the rated value (≈15%), due to the final design choice of using a consequent-pole configuration with bonded NdFeB PMs.

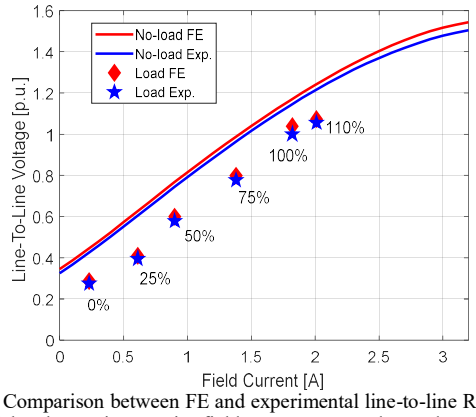

Fig. 13. Comparison between FE and experimental line-to-line RMS voltages provided by the exciter vs. its field current at rated speed: no-load curves (continuous lines); on-load results at various loading levels for the MA with p.f. 0.8 inductive (diamonds and stars).

TABLE III
Comparison between FE and Experimental Results for the MA No-Load Operation

	Exciter $I_{field}= 0A_{dc}$		Exciter $I_{field}= 0.23A_{dc}$	
	I_{f_MA} $[A_{dc}]$	V_{ac_MA} $[V_{rms}]$	I_{F_MA} $[A_{dc}]$	V_{ac_MA} $[V_{RMS}]$
Simulation	10.1	342	14.1	406
Test	9.5	340	13.8	400
Error	5.9%	0.6%	2.1%	1.5%

VI. CONSIDERATIONS

The first benefit of the hybrid exciter concept vs. the benchmark machine consists in the reduction of the m.m.f. required to its field winding. A full performance comparison between benchmark and hybrid exciters based on experimental data is reported in Table IV for several significant operating conditions. For both platforms, the tests are run at cold conditions, due to their short duration starting from room temperature. As expected, the field current is significantly reduced in the hybrid exciter, with a decreasing benefit as the machine load level increases. However, an appreciable improvement is obtained even at 110% of rated load. When the resistance of the field winding is assumed to be the same for both machines, the related Joule losses are then reduced accordingly, as highlighted in Table IV.

The reliability of the considered genset would be significantly improved when the proposed hybrid exciter was

used. In fact, in case of full failure zeroing the exciter field current, the benchmark genset would go out of service whereas in the hybrid version the MA would still be able to supply the load, thanks to the excitation provided by the PMs. In addition, the lower temperature expected in the exciter field winding would affect favorably the reliability of this part and ultimately of the machine, possibly turning into a longer lifetime. Moreover, the reduction of the maximum current required for the field winding may permit to reduce the AVR stress.

TABLE IV
Performance comparison for MA On-Load Operation

Loading % @ p.f. 0.8	Exciter Field Current $I_{f\ exc}$ [A]			Exciter Field Loss Reduction
	Benchmark	Hybrid	Reduction	
0%	0.64	0.23	64.1%	87.1%
25%	0.81	0.61	24.7%	43.3%
50%	1.21	0.90	23.8%	44.7%
75%	1.68	1.38	17.9%	32.5%
100%	2.21	1.82	17.7%	32.2%
110%	2.38	2.01	15.6%	28.7%

The loss reduction in the exciter field winding also increases its efficiency and thus ultimately that of the whole genset. Despite the latter figure would exhibit a numerical improvement that would appear modest due to the much larger size of the MA, the reduction of the exciter losses can result in not-negligible operational and economic advantages, especially in a long-term perspective. In fact, even a limited reduction of losses could provide appreciable cumulated benefits along the entire lifetime of the genset, especially when long periods of continuous operation are expected, such as for the considered industrial case study.

Another important benefit of the proposed hybrid exciter is the improved voltage build-up at start-up. In fact, since the AVR is fed by the MA output, the benchmark genset relies only upon the residual magnetism in the cores to self-excite. On the other hand, in the hybrid exciter, the PMs provide a basic excitation level even at null field current, thus ensuring a fast and reliable voltage build-up as soon as the genset is sped-up.

The main potential drawback deriving from adopting a hybrid excitation solution for the exciter consists in the higher manufacturing cost due to the inclusion of PMs. However, the proposed solution minimizes the modifications of the existing design, and the real impact of any related extra cost could be mitigated or even overcompensated by the energy savings produced during the lifecycle of the genset.

VII. Conclusions

In this paper, the application of hybrid PM – field winding solutions for the excitation of the main exciters of classical self-powered brushless ESs for WFSGs has been proposed and analyzed. The key concept of such solution consists in introducing PMs to provide a suited basic flux level in the exciter even when the field current in the exciter is null. This results then into a boost that adds-up to the field winding m.m.f. during any other operating condition of the MA, still permitting the AVR to control the genset operation via the field current.

As a case study, the proposed concept was applied to an available industrial 400*kVA* genset. The minimization of the impact on the manufacturing process of the existing exciter, on the AVR and on the overall upgrade cost was assumed as a stringent constraint in the design exercise for a potentially more realistic/industrial perspective. After some design iterations, a consequent-pole layout was adopted. A prototype of the designed solution was then built by modifying the exciter of the available genset, gluing the PMs on the gap-facing sides of half of the stator poles that were purposely milled. The genset was then assembled onto a purposely equipped test rig to carry out different tests. The experimental data obtained were compared to the simulation results, confirming the expected operation of the suggested solution, e.g. an excitation loss reduction by 32.2% was achieved at full-load of the MA. Therefore, the hybrid excitation concept was proved to be applicable to brushless exciters of industrial gensets, with multiple appreciable benefits and a minimal impact on their manufacturing process.

References

[1] A. E. Bell, P. Anpalahan, "Optimization of Salient-Pole Rotor for Synchronous Generators," *2018 IEEE XIII International Conference on Electrical Machines (ICEM)*, pp. 339-344, 2018.

[2] S. Nuzzo, P. Bolognesi, G. Vakil, D. Fallows, C. Gerada, N. L. Brown, M. Galea, "A methodology to remove Stator Skew in Small-Medium Size Synchronous Generators via innovative damper cage designs," DOI 10.1109/TIE.2018.2864699, *IEEE Transactions on Industrial Electronics*, 2018.

[3] A. Tessarolo, C. Bassi, D. Giulivo, "Time-stepping finite-element analysis of a 14-MVA salient-pole shipboard for different damper winding design solution," *IEEE Trans. Ind. Electron.*, vol. 59, no. 6, pp. 2524-2535, Jun. 2012.

[4] S. Nuzzo, P. Bolognesi, C. Gerada and M. Galea, "Simplified Damper Cage Circuital Model and Fast Analytical–Numerical Approach for the Analysis of Synchronous Generators," in IEEE Transactions on Industrial Electronics, vol. 66, no. 11, pp. 8361-8371, Nov. 2019.

[5] J G. Klempner; I. Kerszenbaum, "Operation and Control," in Handbook of Large Turbo-Generator Operation and Maintenance, IEEE, 2018, doi: 10.1002/9781119390718.ch4.

[6] S. Nuzzo, M. Galea, C. Gerada, and N. L. Brown, "Prediction of the voltage drop due to the diode commutation process in the excitation system of salient-pole synchronous generators," *19th International Conference on Electrical Machines and Systems (ICEMS)*, pp. 1–6, 2016.

[7] S. Nuzzo, M. Galea, C. Gerada, N. Brown, "Analysis, modelling and design considerations for the excitation systems of synchronous generators," *IEEE Transactions on Industrial. Electronics*, vol. 65, no. 4, pp. 2996-3007, Apr. 2018.

[8] G. Laliberte, "A comparison of generator excitation systems (Power topic 6008-Technical information from Cummins Power Generation)," in *Technical Report GLPT-6008-EN (10/14)*, Oct. 2014, pp. 1–6.

[9] J. K. Nøland, S. Nuzzo, A. Tessarolo and E. F. Alves, "Excitation System Technologies for Wound-Field Synchronous Machines: Survey of Solutions and Evolving Trends," in *IEEE Access*, vol. 7, pp. 109699-109718, 2019.

[10] J. F. Gieras, "PM synchronous generators with hybrid excitation systems and voltage control Capabilities: A review," 2012 XXth International Conference on Electrical Machines, Marseille, 2012, pp. 2573-2579.

[11] J-C. Matt, J-C. Mipo, A. Foggia, "Synchronous Rotary Electric Machine having a Hybrid-Excitation Rotor", U.S. 9,197, 118 B2, 2015.

[12] M. Onsal, Y. Demir and M. Aydin, "A New Nine-Phase Permanent Magnet Synchronous Motor With Consequent Pole Rotor for High-Power Traction Applications," in *IEEE Transactions on Magnetics*, vol. 53, no. 11, pp. 1-6, Nov. 2017, Art no. 8700606.

[13] H. Hua, Z. Q. Zhu, H. Zhan, "Novel Consequent-Pole Hybrid Excited Machine with Separated Excitation Stator," *IEEE Trans. on Ind. Electron.*, vol. 63, no. 8, pp. 4718–4728, 2016.

[14] J. Pyrhonen, J. Tapani, and V. Hrabovcova,` Design of Rotating Electrical Machines. Chichester, U.K.: Wiley, 2008.

[15] P. Bolognesi, "A mid-complexity analysis of long-drum-type electric machines suitable for circuital modelling," *Proc. of ICEM 2008 Conf.*, Vilamoura, Sep. 2008.